New evidence of meteoritic origin of the Tunguska cosmic body

Victor Kvasnytsya[a], Richard Wirth[b], Larissa Dobrzhinetskaya[c], Jennifer Matzel[d], Benjamin Jacobsen[d], Ian Hutcheon[d], Ryan Tappero[e], Mykola Kovalyukh[f]

a Institute of Geochemistry, Mineralogy and Ore Formation of National Academy of Sciences of Ukraine, Palladin Avenue 34, 03680 Kyiv-142, Ukraine

b Helmholtz-Centre Potsdam, German Research Centre for Geosciences, GFZ, Telegrafenberg, 14473 Potsdam, Germany

c Department of Earth Sciences, University of California at Riverside, Riverside, CA 92521, USA

d Lawrence Livermore National Laboratory, Livermore, CA 94550, USA

e Brookhaven National Laboratory, Upton, NY 11973, USA

f Institute of Environmental Geochemistry of National Academy of Sciences of Ukraine, Palladin Avenue 34a, 03680 Kyiv-142, Ukraine

Corresponding author:
Prof. Victor Kvasnytsya
Institute of Geochemistry, Mineralogy and Ore Formation,
National Academy of Sciences of Ukraine,
Palladin Ave., 34
03680 Kyiv-142
Ukraine
Phone 0038 (044) 424 05 40
Fax 0038 (044) 424 12 70
e-mail: vmkvas@hotmail.com

Abstract

Diamond-lonsdaleite-graphite micro-samples collected from peat after the 1908 catastrophic blast in the Tunguska area were studied with scanning (SEM) and transmission electron (TEM) microscopy, NanoSecondary Ion Mass Spectrometry (NanoSIMS) and X-ray synchrotron technique. The high-pressure carbon allotropes in the Tunguska samples are being described for the first time and contain inclusions of FeS (troilite), Fe-Ni (taenite), γ-Fe and $(FeNi)_3P$ (schreibersite). The samples are nodule-like in shape and consist of 99.5% carbon minerals, e.g. diamond > lonsdaleite > graphite. Micro- and nanoinclusions of troilite (up to 0.5 vol. %), taenite, γ-iron and schreibersite fill cracks, cleavages and pores in the carbon matrix. Carbon isotope studies from the two analyses of the Tunguska foil showed $\delta^{13}C$ = -16.0 +/- 1.9‰ and $\delta^{13}C$ = -15.2 +/- 2.1 ‰, suggesting $\delta^{13}C$ = -15.6 +/- 2‰ as an average characteristic of the carbon reservoir. That value is close to $\delta^{13}C$ of some extraterrestrial samples. A negligible concentration of Ir and Os in the carbonaceous matrix promotes some controversial interpretation of the origin of the studied materials. Attributing this fact to the primary inhomogeneity, and considering the micro-structural features such as cracks, deformation of the crystal lattices, etc coupled with high-pressure carbon allotropes association with metals, sulfides and phosphides, and the high ratio of Fe:Ni = 22:1 suggest that the studied samples are meteorite micro-remnants.

Key words: diamond, lonsdaleite, graphite**,** troilite, taenite, γ-iron, schreibersite, intergrowths, meteorite, Tunguska area

1. Introduction

The extremely powerful Tunguska blast of an unknown extraterrestrial object occurred at June 30, 1908 near the river of Podkamennaya Tunguska (60°54'07"N 101°54'16"E) in an unpopulated part of Siberia, Russia. The blast was estimated to be equivalent to 3-5 megatons of trinitrotoluene (e.g. Boslough, Crawford, 2008), and it burned and flattened taiga forests over an area >2000 km^2. The origin of the Tunguska blast was explained by a huge meteorite impact (e.g. Yavnel, 1957; Florensky, 1963; Longo et al., 1994; Serra et al., 1994; Longo, 2007; Gasperini et al., 2007, 2009; Badyukov et al., 2011) or by a comet (e.g. Florensky, 1968 a, 1968 b; Golenetsky et al., 1977; Ganapathy et al., 1983; Zbik, 1984; Nazarov et al., 1990; Hou et al., 1998; Kolesnikov et al., 1999; Rasmussen et al., 1999; Kolesnikov et al., 2003, 2005; Gladysheva, 2007), or by a cosmic body. However, no clear differences between comet and meteorite impacts were established (Dolgov et al, 1973; Nazarov et al., 1983; Hou et al., 2000; 2004; Kolesnikov et al., 2005). A less-supported concept of a deep plume originating from the lower most mantle, which 'penetrated' the lithospheric plate beneath Siberia and escaped to the atmosphere causing a gigantic blast in the Tunguska vicinity, was recently proposed (Skublov et al., 2011). Geochemical data from the natural materials in the epicenter of the Tunguska blast sometimes fit well to either a comet blast or meteorite impact (iron or chondritic), in many other cases researchers cannot separate meteoritic characteristics from those that

would refer to a comet. The problem of this uncertain interpretation is that no large fragments of meteorite were ever identified in the Tunguska blast area. The interest to Tunguska was renewed a decade ago after new samples were collected in the vicinity of Lake Cheko, which was proposed to be a filled impact crater formed at the time of the Tunguska event (Gasperini et al., 2007). The meteorite impact crater hypothesis of Gasperini et al. (2007) was rejected by Collins et al. (2008). Later Gasperini et al. (2009) provided more evidence that the crater of interest was formed at the time of the Tunguska event.

In this context we continue to study Tunguska samples that are available in the archives of the Institute of Geochemistry and Mineral Physics of the Academy of Sciences (Ukraine), and are using new high-resolution analytical and imagining techniques. These samples were collected and documented in 1978 during scientific expeditions organized and financed by the Academy of Sciences of the former Ukrainian SSR. Using high resolution scanning (SEM) and transmission electron microscopy (TEM), focused ion beam (FIB) technique for TEM sample preparation, Nano-secondary ion mass-spectrometry (NanoSIMS) and synchrotron-based X-ray microfluorescence beam technique, we have studied several small samples of carbon-bearing materials from the Tunguska epicenter.

2. Previous work

Studies carried out in early 1979-1980's showed that peat samples from the Tunguska site include 'amalgamated' polycrystalline micro-aggregates of diamond, lonsdaleite, graphite and troilite (Table 1) which contain traces of Co, Ni, Cr, Rb, Cs, Sr, Ba, Sc, Zr, Ir, Th, Hf, La, Ce, Nd, Sm, Eu, Tb, Yb, Rb, Fe, S,

Si and Al (e.g. Kvasnitsa et al., 1979; 1980; Sobotovich et al., 1980, 1985). While concentrations of La, Ce, Sm, Eu, Tb, Yb and others corresponded to the normal background known for terrestrial rocks, elevated ratios of Ni/Co=26 together with high-pressure allotropes of carbon and troilite were interpreted as possible remnants of a meteorite and products of shock metamorphism (Kvasnitsa et al., 1979, 1980). However, Sobotovich et al. (1985) suggested that the diamond-lonsdaleite carbon allotropes enriched in diverse trace elements are products of the shock metamorphism of the terrestrial graphite available on the Earth's surface during the Tunguska blast or even outside the context of the Tunguska event.

Sobotovich at al. (1985) strongly strengthened their conclusions based on the fact that the Ir concentration (0.16 ppm) in the Tunguska diamond-lonsdaleite-graphite intergrowths is five times smaller than that in meteorites. Moreover, in support of Sobotovich et al.'s hypothesis, later Hough et al. (1995) confirmed that chemically robust carbon particles in peat from the Tunguska blast area do not contain any extraterrestrial signatures, because their isotopic signature $\delta^{13}C$=-25‰, and $\delta^{15}N$=0‰ correspond to those of organic matter. However, though all mentioned evidences are correct, some uncertainties remain in Sobotovich et al.'s interpretation because the Ir content in the Tunguska diamond-lonsdaleite-graphite intergrowths is about 10 times larger than that in the terrestrial rocks.

3. Samples and analyses

In this paper we present results of our studies of five fragments of several grains of diamond-lonsdaleite-graphite intergrowths found in peat collected from

the Northern peat bog near Kulik's izba situated close to the Tunguska blast epicenter (Fig. 1). The sample of the peat was selected from the $3m^2$ area. Composition of the peat does not depend on the chemical composition of the underlying rocks, so moss (Sphagnum fuscum) - oligotorf gets minerals from the air as a result of loss of aerosols. Layers of peat, which include the catastrophic layer 1908, depending on the terrain, were collected from a depth of 22-44 cm. The peat is simply stratified, which helps to identify a layer of peat from the year 1908. This peat layer is strongly enriched in silicate and magnetite spherules. The 1908 peat layer near the Northern peat bog is located at a depth of 39-42 cm below the surface; the thickness of the layer is up to 3 cm; unfortunately the age data were not available from that site.

Minerals included in the peat layer of 1908 were separated by washing. The peat was soaked in enamel containers and the organic component was removed. The total amount of the concentrate was 73 grams, 14 grams of which were gray concentrate. The latter was divided into five heavy liquid fractions. In one of the heavy fractions a few solid grains 0.2-0.8 mm in diameter were found. X-ray study of these grains showed that they are diamond-lonsdaleite-graphite intergrowths (Table 1). In this fraction numerous small colorless and green grains of moissanite were identified. They are moissanite polytypes a-SiC 15R and a-SiC 6H respectively (Kvasnitsa et al., 1979).

Each fragment (<0.5mm) of the diamond-lonsdaleite-graphite intergrowths is black with a dull surface luster. They are represented by apographitic impact diamonds that are formed on micro-aggregates of graphite (not on single crystals of graphite). Three fragments of such diamond-

lonsdaleite-graphite intergrowths were studied with SEM and two of them with TEM followed by NanoSIMS and X-ray synchrotron technique.

The SEM studies were performed at the Institute of Geochemistry, Mineralogy and Ore Formation of NAS, Kyiv, Ukraine, using a JSM-6700 F instrument equipped with an energy dispersive X-ray system JED-2300 (JEOL, Japan).

The TEM studies were performed at GFZ, Potsdam, Germany using a Tecnai F20 X-Twin electron microscope equipped with Gatan Tridiem electron energy-loss (EELS) spectrometer, a high-angle annular dark field (HAADF) detector and energy-dispersive X-Ray detection (EDX) system. TEM methods include high-resolution electron microscopy (HREM), selected area electron-diffraction (SAED), calculated electron diffraction pattern (FFT) from high-resolution images, diffraction contrast imaging, analytical electron microscopy *(*AEM) and electron energy-loss spectroscopy (EELS). The chemical composition of the inclusions was determined by analytical electron microscopy (AEM) in the scanning transmission (STEM) mode. Acquisition time usually was 60 seconds. Data evaluation was performed by applying the TIA software package. The d-spacing (d_{hkl}) of the matrix phases and some inclusions was determined from the HREM images and resulting fast Fourier Transforms (FFT) as well as electron diffraction patterns analysis. EEL spectroscopy was applied to distinguish between diamond/lonsdaleite (sp^3 bonding) and graphite (sp^2 bonding).

The samples for TEM study, ultrathin foils of dimension ca. 15x10x0.2 micrometer, were prepared using the single beam FEI FIB 200 focused ion beam

(FIB) device at GFZ Potsdam. Six foils were cut from two different samples. The details of the FIB methods are described elsewhere (e.g. Wirth, 2004, 2009).

Secondary Ion Mass Spectrometry (SIMS) studies of FIB foils were performed at the Lawrence Livermore National Laboratory (USA) using a Cameca NanoSIMS 50 instrument. A ~0.5 pA Cs^+ primary beam was focused to a nominal spot size of ~80 nm and rastered over the sample in 64 × 64 pixel arrays to generate secondary ions. The dwell time was 2 ms/pixel, and the raster size was 3 μm^2. The secondary ion mass spectrometer was tuned for a mass resolving power of ~6500 to resolve isobaric interferences. Negative secondary ions ($^{12}C_2^-$, $^{12}C^{13}C^-$, $^{12}C^{14}N$-, $^{12}C^{15}N^-$, and $^{28}Si^-$) were detected in simultaneous collection mode by pulse counting to generate 1000 serial quantitative secondary ion images (i.e. layers) per analysis. The data were corrected for instrumental mass-dependent fractionation of C and N based on analyses of an in-house *Bacillus subtilis* endospore sample of known $\delta^{13}C$ and $\delta^{15}N$. The data were processed as quantitative isotope ratio images by using custom software (L'Image by Larry Nittler) and were corrected for detector dead-time, image shift from layer to layer and quasi-simultaneous arrival of ions (QSA). Regions of interest were defined based on comparison with TEM images and the isotopic composition for each region was calculated by averaging over the replicate layers. The errors for $\delta^{13}C$ are 2SD. They are extrapolated from the internal error that is based on the counting statistics for each individual analysis and the external error, which is the reproducibility of the standards.

Synchrotron-based X-ray microfluorescence (μSXRF) images of the sample were acquired from Beamline X27A of the National Synchrotron Light Source (NSLS) at Brookhaven National Laboratory (Upton, NY, USA) (Ablett et al., 2006). This bend-magnet beamline uses Kirkpatrick-Baez (K-B) mirrors to produce a focused spot (7 by 14 μm) of hard X-rays with tunable energy achieved via Si (111) or Si (311) channel-cut monochromator crystals. For μSXRF imaging, the incident beam energy was fixed at 11.5 keV to excite all target elements simultaneously. The sample was oriented 45° to the incident beam, and rastered in the path of the beam by an XY stage while X-ray fluorescence was detected by a 13-element Canberra Ge array detector oriented 90° to the incident beam. Elemental maps were collected from a 0.25 mm^2 sample area using a step size of 10 μm and a dwell time of 300 seconds. The fluorescence yields were normalized to the changes in intensity of the X-ray beam (I_0) and the dwell time. Data acquisition and processing were performed using IDL-based beamline software designed by CARS (The University of Chicago, Consortium for Advanced Radiation Sources) and NSLS Beamline X26A (data analysis software available at http://www.bnl.gov/x26a/comp_download.shtml). Each pixel of the μSXRF image has a discrete energy-dispersive spectrum (EDS). Peak fitting of the EDS can be used to resolve spectral overlaps, such as the overlap of Ir Lα1 with Ga Kα, or the overlap of Os Lα1 with Cu Kβ. The sample had been milled with a Ga+ ion beam, and therefore had a significant amount of Ga implanted on its surface. The presence of Ga creates a challenge for the trace detection of Ir

fluorescence. Likewise, the sample was supported on a disc of brass (Cu-Zn alloy), and the presence of Cu creates a challenge for the trace detection of Os fluorescence. Also, Cu was detected in the sample itself. An EDS from a pixel with relatively low Ga and Cu counts was extracted from the image for peak fit analysis. For the determination of the relative Fe/Ni ratio, we used a fundamental parameters (FP) approach where the relationship between concentration and fluorescence intensity was determined with standards; FP algorithms were used to correct for matrix effects. The imperfection of such determination is ±0.37 for Fe (wt%) and ±0.02 for Ni (wt%).

4. Results

4.1. SEM study

The studied fragments are characterized by "chondrule-like" shape with "lamellar-like" platy microstructures (Fig.2) which obliterate the microporosity observed on the samples surface. The secondary electron images (Fig.3) show a fragment of three intergrown allotrops of carbon (diamond, lonsdaleite and graphite), which contain particles of troilite (crystals, plates and films). The frequency of occurrence of the three different phases is as follows: diamond > lonsdaleite > graphite > troilite. The chemical composition of the individual particles of troilite is very similar; the average of 9 analyses with SEM-EDAX system is (wt %): Fe=62.13; S=33.0; Cr=1.16; Cu=3.22.

4.2. TEM study

The area of all studied foils (e.g. Fig.4a) consists of 99.5 % of carbon minerals. A series of cracks, contortion and fragmentation zones (Fig.4 b, c, d) are observed in the foils; they can be interpreted as traces of shock compression

of the samples. Inclusions of other minerals are situated in the vicinity of the shock deformation features.

Carbon allotropes (diamond, lonsdaleite, graphite). In X-ray diffraction pattern analysis a series of broadened scattering intensities indicating the presence of graphite, lonsdaleite and diamond can be distinguished (Kvasnitsa et al., 1979). The difference in relative scattering intensities indicates that the phases are present in different concentrations, but mostly the frequency of occurrence is in the following sequence: diamond > lonsdaleite > graphite (Table 1). The X-ray study suggests that the average grain size of the phases mentioned above is in the range of 10-100 nm. This is confirmed by dark-field images from the foils (Fig. 4 d) showing fine polycrystalline aggregates composed of grains of the carbon minerals up to 0.5 micron size.

In contrast, electron diffraction patterns of all six foils studied show that they consist of crystallites of lonsdaleite and graphite (Fig. 5 a). The selected area diffraction pattern represents a larger volume of the foil (approximately 5 micrometer in diameter). Most frequently the observed d-spacing d_{hkl} belongs to lonsdaleite (2.167 nm, 2.07 nm, 1.93 nm, 1.25 nm, 1.16 nm,) and graphite (3.30 nm, 3.25 nm, 1.68 nm) (Table 2). For comparison, we present an image of electron diffraction pattern of the carbon phases (with lonsdaleite predominanting) of apographitic impact diamond from Popigai crater, Russia (fig. 6).

Inverse FFT`s of filtered HREM images show the presence of lonsdaleite + diamond on a nanometre scale (Fig.5 b). EEL spectra show only sp^3 bonding in

both diamond and lonsdaleite (Fig.5 c). Locally the lonsdaleite and diamond layers intersect each other, but mainly diamond crystallites are present as small particles irregularly neighboring the lonsdaleite crystals. The size of the carbon grains varies from 5 to 15 nm, however, occasionally diamond crystallites up to 30 nm, lonsdaleite up to 20 nm and graphite up to 40 nm in size can be observed. For most of the crystals, especially those of graphite, deformation such as bending of the layers, and their discontinuity or dislocations are intrinsic.

Inclusions of FeS (troilite), Fe-Ni (taenite), γ-Fe and $(FeNi)_3P$ (schreibersite). Numerous inclusions of iron monosulfide of various shape, dimension and localization were found in each of the foils (Fig.7 a, b). Their relatively large aggregates containing crystals of imperfect shape (300 - 750 nm in size) are located in the carbon matrix. Aggregates of troilite grains (30-50 nm in size) are accumulated within cracks in the carbon allotropes matrix. Microveins (2 μm long and 10-30 nm wide) composed of troilite are also observed within the foils.

In foil #2504 we detected troilite, with approximately stoichiometric composition. Its average composition calculated from 11 measurements is close to that measured by SEM with the exception of Cu (wt %): Fe=61.77; S=36.95; Cr=1.23; Ni=0.51. We cannot reliably measure Cu concentrations in the sample with EDS-TEM system because Cu X-ray intensity is always present in the spectra caused by the Cu-grid the TEM foil rests on. Troilite often is associates with taenite, γ-Fe and schreibersite nanoinclusions, which are found together within cracks (Fig.8). Figs. 9a & b show a 500 nm inclusion of FeS with low chromium concentration; the diffraction pattern suggests that this FeS is

pyrrhotite (Fig.9 c). No difference in composition between different aggregates of troilite and their location in the matrix was observed.

Nanoinclusions of taenite (25-50 nm in size) (Fig. 10) have a chemical composition in wt. % (average of 3 measurements): Fe =78.45 and Ni =21.55 (Table 3). Frequently taenite forms intergrowths (up to 100 nm in size) with troilite and schreibersite. Taenite aggregations are built of irregular grains and plates. Rare irregular nanograins of γ-iron ($a_{0=}$0.356 nm) are intergrown with taenite (Fig. 11). Individual grains of schreibersite (Fig. 12) in nano-aggregations are approximately 20-30 nm in size. Its chemical composition is variable with an average of 3 measurements (in wt. %): Fe – 64.77, Ni – 18.94, P – 16.29.

Submicrometer-sized grains (up to 350 nm) of aragonite were found in foil #2523. Aragonite was confirmed with both EDS and electron diffraction patterns.

4.3. NanoSIMS study

Carbon isotope studies from the two analyses of the Tunguska foil showed $\delta^{13}C$ = -16.0 +/- 1.9‰ and $\delta^{13}C$ = -15.2 +/- 2.1 ‰, giving $\delta^{13}C$ = -15.6 +/- 2‰ as the average number for the carbon reservoir. This data is fractionation corrected using a spore sample of known isotopic composition (see references in Dobrzhinetskaya et al., 2009). Nitrogen concentration was too low to be accurately measurable.

4.4. Synchrotron-based X-ray microfluorescence (μSXRF) image analyses

Osmium abundance in the Tunguska sample was too low to be detected with synchrotron-based X-ray microfluorescence at Beamline X27A. Thus, its presence measured earlier could not be confirmed. Iridium abundance, albeit very close to the detection limit, was detectable from the sample; a spectral contribution from Ir Lα1 was necessary to accurately model the energy-dispersive spectrum. The EDS indicates the sample has a Fe:Ni concentration ratio of approximately 22:1 (Fe = 38.90 wt% and Ni = 1.80 wt%).

5. Discussion and Conclusions

This study shows that the Tunguska samples consist of three allotropes of carbon, diamond > lonsdaleite > graphite with an average carbon isotopic ratio $\delta^{13}C$ = -15.6 +/- 2‰. We observed that nanoinclusions of troilite, taenite, γ-Fe and schreibersite in the carbonaceous matrix associate with cracks, pores, or extend out from single grains of troilite as tiny veins. We speculate that these minerals were formed by impregnation of melt into solid carbonaceous matrix crystallizing during rapid cooling. Therefore, such iron-nickel-sulfide-phosphide mineralization could be the product of condensation of vapor originating from overheated impact melt which penetrated through cracks, pores and into carbon material (former graphite). Bulk chemistry of mineral inclusions in the carbonaceous matrix is close to quadruple eutectics Fe-Ni-S-P with considerable nickel content. This is obvious in most EDS spectra of nanoinclusions (e.g., Fig. 8), and it suggests that a mixture of metal, sulfide and phosphide phases, together with their fine intergrowths occurred during rapid cooling. Crystallization of such an association in the Cape York iron meteorite, for instance (Esbensen and Buchwald, 1981), occurred at the temperature range

1475-700°C. The presence of taenite, stable at temperature 1400-920°C (Kubaschewski, 1982) and γ-Fe in the Tunguska samples suggests their high temperature crystallization, whereas the presence of diamond and lonsdaleite indicates a high-pressure environment. It is well known that nanocrystalline γ-Fe is stable at ambient conditions and does not transform into α-Fe, which is stable at room temperature (Gleiter, 1989). According to the carbon stability field diagram (Bundy, 1980) graphite can co-exists with diamond at T = 1400-900°C and P = 7-5 GPa, whereas the stability boundary between diamond-graphite and lonsdaleite are still unknown. Thus, the collected data together with measurements suggests that the studied Tunguska samples most likely represent small remnants of an iron meteorite, which is also strongly supported by the high ratio of Fe:Ni = 22:1 and Ni/Co =26 (Sobotovich et al., 1985). On the other hand, some controversial data, such as the low Iridium and Osmium contents, which are close to the detection limit, the presence of aragonite and a light carbon ($\delta^{13}C$ = -15.6 +/- 2‰) reservoir might suggest that the precursor of the studied Tunguska samples was terrestrial carbon material (graphite). Although the $\delta^{13}C$ value of the Tunguska samples is similar to that of some iron meteorites, e.g. graphite nodule of Kendall County hexahedrite ($\delta^{13}C$ = -13.3 to -14.50 ‰; Deines and Wickman, 1973, 1975), the negligible content of Os and Ir in the carbon matrix would support its terrestrial precursor.

However, ignoring negligible contents of Ir and Os (which may be due to primary inhomogeneity), and taking into account the presence of native metal, sulfide and phosphide (e.g. troilite, taenite, γ-iron and schreibersite) in diamond-

lonsdaleite-graphite matrix, we conclude that the studied Tunguska samples are microscopically small remnants of a meteoritic body.

The association of high-pressure carbon allotropes, diamond and lonsdaleite, with troilite, taenite, γ-Fe and schreibersite is established for the first time in the Tunguska samples. Almost the same association of minerals was found in iron meteorites of Canyon Diablo, ALHA 74-283, Magura and Chuckwalla (e.g. Ksanda and Henderson, 1939; Lipschutz and Anders, 1961; Carter and Kennedy, 1964; El Coresy, 1965; Anders and Lipschutz, 1966; Heymann et al., 1966; Hanneman et al., 1967; Frondel and Marvin, 1967; Clarke et al., 1981; Garvie and Nemeth, 2009) and in many ureilites (e.g. Urey et al., 1957; Lipschutz, 1962, 1964; Vdovykin, 1970; Valter et al., 2003; Karczemska et al., 2009). While diamond and lonsdaleite were considered to be products of the impact, other metallic phases such as troilite, schreibersite, γ-Fe and taenite were described as a typical set of meteoritic minerals.

For additional confirmation of the meteoritic nature and more definite determination of the meteorite type, investigations of $^{3}He/^{4}He$ ratio, xenon isotopes ($^{136}Xe/^{130}Xe$ and $^{129}Xe/^{130}Xe$), noble gases, rear earth elements and PGE contents should be carried out.

Aknowledgments

VK thanks the German Science Foundation (DFG), Bonn-Bad Godesberg for a travel grant. Part of this research conducted in the Lawrence Livermore National Laboratory was supported by LAB-FEE Research Grant (to LD-JM-BJ-IH). The work performed at Beamline X27A, National Synchrotron Light Source (NSLS) of the Brookhaven National Laboratory. It was supported in part by the U.S. Department of Energy - Geosciences (DE-FG02-92ER14244 to The University of Chicago - CARS). Use of the NSLS was supported by the U.S.

Department of Energy, Office of Science, Office of Basic Energy Sciences, under Contract No. DE-AC02-98CH10886. A. Schreiber (GFZ Potsdam) is thanked for the TEM sample preparation with FIB. Thanks to M. M. Taran for useful advices and discussion. We also thank anonymous reviewers and Felix Kaminsky for helpful criticism that significantly improved the manuscript.

References

Ablett, J.M., Kao, C.C., Reeder, R.J., Tang, Y., Lanzirotti, A., 2006. X27A - a new hard X-ray micro-spectroscopy facility at the National Synchrotron Light Source. Nuclear Instruments and Methods in Physics Research A 562, 487-494.

Anders, E., Lipschutz, M.E., 1966. Critique of paper by N.L.Carter and G.C.Kennedy "Origin of diamonds in the Canyon Diablo and Novo Urei meteorites". J. Geoph. Research 71**,** 643-661.

Badyukov, D.D., Ivanov, A.V., Raitala, J., Khisina, N.R., 2011. Spherules from the Tunguska event site: Could they originate from Tunguska cosmic body? Geokhimiya 7**,** 675-689 (in Russian).

Boslough, M.B.E., Crawford D.A., 2008. Low-altitude airbursts and the impact threat. Inter. J. Impact Engineering 35, 12, 1441–1448.

Bundy, F.P., 1980. The P, T phase and reaction diagram for elemental carbon, 1979. J. Geoph. Research 85, 6930-6936.

Carter, N.L., Kennedy, C.G., 1964. Origin of diamonds in the Canyon Diablo and Novo Urei meteorites. J. Geoph. Research 69**,** 2403-2421.

Clarke, R.S., Appleman D.E., and Ross D.R., 1981. An Antarctic iron meteorite contains preterrestrial impact-produced diamond and lonsdaleite. Nature 291**,** 396-398.

Collins G.S., Artemieva, N., Wunnemann, K., Bland, P.A., Reimold, W.U., Koeberl, C., 2008. Evidence that Lake Cheko is not an impact crater. Terra Nova 20**,** 165–168.

Deines, P., Wickman, F. E., 1973. The isotopic composition of ''graphitic'' carbon from iron meteorites and some remarks on the troilitic sulfur of iron meteorites. Geochim. Cosmochim. Acta 37**,** 1295-1319.

Deines, P., Wickman, F. E., 1975. A contribution to the stable carbon isotope geochemistry of iron meteorites. Geochim. Cosmochim. Acta 39**,** 547-557.

Dobrzhinetskaya, L. F., Wirth, R., Yang, J., Hutcheon, I.D., Weber, P., Green, H.W., 2009. Nitrides and oxides recording a highly reduced mantle environments form an ophiolite. PNAS Unit. St. Am. 106, 19233-19238.

Dolgov, Yu.A., Vasil'yev, N.V., Shugurova, N.A., Lavrent'yev, Yu.T., Grishin, Yu.A., L'vov, Yu.A., 1973. Composition of microspherules from peats at the place of the fall of Tunguska meteorite. Meteoritika 32**,** 147-149 (in Russian).

El Coresy, A., 1965. Mineralbestand und Structuren der Graphit – und Sulfideinschlüsse in Eisenmeteoriten. Geochim. Cosmochim. Acta 29**,** 1131-1151.

Esbensen, H.K., Buchwald, F.V., 1981. Late crystallisation of the natural Fe-Ni-S-P System – Evidence from Cape York troilite inclusions. Meteoritics 16**,** 313.

Florensky, K.P., 1963. Previous results of the Tunguska meteoritic complex exspedition of 1961. Meteoritika 23**,** 3-29 (in Russian).

Florensky, K.P., Ivanov, A.V., Ilyin, N.P., Petrikova, M.N., Loseva, L.E., 1968a. Chemical composition of cosmic spherules from the region of the Tunguska disaster and some problems of the differentiation of cosmic body material. Geokhimiya 10**,** 1163-1173 (in Russian).

Florensky, K.P., Ivanov, A.V., Kirova, O.A., Zaslavskaya, N.I., 1968b. Phase composition of finely dispersed extraterrestrial material from the region of the Tunguska disaster. Geokhimiya 10**,** 1174-1182 (in Russian).

Frondel, C., Marvin, B.U., 1967. Lonsdaleite, a hexagonal polymorph of diamond. Nature 214**,** 587-589.

Ganapathy, R., 1983. The Tunguska Explosion of 1908: Discovery of meteoritic debris near the explosion site and at the South Pole. Science 220**,** 1158-1161.

Garvie, A.J.L., Nemeth, P., 2009. The structure of Canyon Diablo "diamonds". 40-th Lunar Planet. Sci. Conf. 1346 (pdf).

Gasperini, L., Alvisi, F., Biasini, G., Bonatti, E., Longo, G., Pipan, M., Ravaioli, M., Serra, R., 2007. A possible impact crater for the 1908 Tunguska event. Terra Nova 19**,** 245-251.

Gasperini, L., Bonatti, E., Albertazzi, S., Forlani, L., Accorsi, C.A., Longo, G., Ravaioli, M., Alvisi, F., Polonia, A., Sacchetti, F., 2009. Sediments from Lake Cheko (Siberia), a possible impact crater for the 1908 Tunguska Event. Terra Nova 21**,** 489–494.

Gladysheva, O.G., 2007. On the Problem of the Tunguska Meteorite Material. Solar System Research 41, 314-321.

Gleiter, H., 1989. Nanocrystalline Materials. Progress in Materials Science 33, 223-315.

Golenetsky, S.P., Stepanok, V.V., Kolesnikov, E.M., 1977. Signs of cosmochemical anomaly in the area of 1908 year Tunguska catastrophe. Geokhimiya 11**,** 1635-1645 (in Russian).

Hanneman, R.E., Strong, H.M., Bundy, F.P., 1967. Hexagonal diamonds in meteorites: Implications. Science 155**,** 995-997.

Heymann, D., Lipschutz, M.E., Nelson, B., Anders, E., 1966. Canyon Diablo meteorite: metallographic and mass spectrometric study of 56 fragments. J. Geoph. Research 71**,** 619-641.

Hou, Q.L., Kolesnikov, E.M., Xie, L.W., Kolesnikova, N.V., Zhou, M.F., Sun, M., 2004. Platinum group element abundances in a peat layer associated with the Tunguska event, further evidence for a cosmic origin. Planet. Space Sci. 52**,** 331-340.

Hou, Q.L., Kolesnikov, E.M., Xie, L.W., Zhou, M.F., Sun, M., Kolesnikova, N.V., 2000. Discovery of probable Tunguska Cosmic Body material: anomalies of platinum group elements and rare-earth elements in peat near the explosion site (1908). Planet. Space Sci. 48**,** 1447-1455.

Hou, Q.L., Ma, P.X., Kolesnikov, E.M., 1998. Discovery of iridium and other element anomalies near the 1908 Tunguska explosion site. Planet. Space Sci. 46**,** 179-188.

Hough, R.M., Gilmour, I., Newton, J., Arden, J., Pillinger, C.T. 1995. Chemically robust carbon particles in peat from the Tunguska impact site. Meteoritics 30**,** 521.

Karczemska, A., Jakubowski, T., Vergas, F., 2009. Different diamonds in meteorites – DaG868 and NWA 3140 ureilites. J. Achiev. Mater. Manufact. Engineer**.** 37**,** 292-297.

Kolesnikov, E.M., Boettger, T., Kolesnikova, N.V., 1999. Finding of probable Tunguska Cosmic Body material: isotopic anomalies of carbon and hydrogen in peat. Planet. Space Sci**.** 47**,** 905-916.

Kolesnikov, E.M., Hou, Q.L., Xie, L.W., Kolesnikova, N.V., 2005. Finding of probable Tunguska Cosmic Body material: anomalies in platinum group elements in peat from the explosion area. Astronom. Astroph. Transactions 24, 101-111.

Kolesnikov, E.M., Longo, G., Boettger, T., Kolesnikova, N.V., Gioaccihini, P., Forlani, L., Giampieri, R., Serra R., 2003. Isotopic-geochemical study of nitrogen and carbon in peat from Tunguska Cosmic Body explosion site. ICARUS 161**,** 235-243.

Ksanda, C.J., Henderson, E.P., 1939. Identification of diamond in the Canyon Diablo iron. Amer. Mineral. 24**,** 677-680.

Kubaschewski, O., 1982. Iron-Binary Phase Diagrams. Springer-Verlag, Berlin-Heidelberg-New-York.

Kvasnitsa, V.N., Sobotovich, E.V., Kovalyukh, N.N., 1980. Diamond-graphite intergrowths in turfs of Tunguska disaster region. In: Scientific methods of forecast, prospecting and assessment of diamond deposits, Moscow, 57-58 (abstr., in Russian).

Kvasnitsa, V.N., Sobotovich, E.V., Kovalyukh, N.N., Litvin, A.L., Rybalko, S.I., Sharkin. O.P., Yegorova L.H., 1979. High-bar polymorphs of carbon in turfs of Tunguska disaster region. Doklady Akademii Nauk USSR, Seriya B 12**,** 1000-1004 (in Russian).

Lipschutz, M.E., 1962. Diamonds in the Dyalpur meteorite. Science 138**,** 1266-1267.

Lipschutz, M.E., 1964. Origin of diamonds in the ureilites. Science 143**,** 1431-1434.

Lipschutz, M.E., Anders, E., 1961. The record in the meteorites – IV. Origin of diamonds in iron meteorites. Geochim. Cosmochim. Acta 24**,** 83-105.

Longo, G., 2007. The Tunguska event, in: Bobrowsky, P.T., Rickman, H. (Eds.), Comet/Asteroid Impacts and Human Society, An Interdisciplinary Approach. Springer-Verlag, Berlin-Heidelberg, **18,** pp**.** 303–330.

Longo, G., Serra, R., Cecchini, S., Galli M., 1994. Search for microremnants of the Tunguska Cosmic Body. Planet. Space Sci. 42**,** 163-177.

Nazarov, M.A., Korina, M.I., Barsukova, L.D., Kolesnikov, E.M., Suponeva, I.V., Kolesov, G.M., 1990. Material traces of the Tunguska bolide. Geokhimiya 5**,** 627-639 (in Russian).

Nazarov, N.A., Korina, N.I., Kolesov, G.M., Vassil'ev, N.V., Kolesnikov, E.M., 1983. The Tunguska event: mineralogical and geochemical data. Lunar Planet. Sci. Conf. 14**,** 548-549 (abstr.).

Rasmussen, K.L., Olsen, H.J.F., Gwozdz, R., Kolesnikov, E.M., 1999. Evidence for a very high carbon/iridium ratio in the Tunguska impactor. Meteoritics Planet. Sci. 34**,** 891-895.

Serra, R., Cecchini, S., Galli, M., Longo, G., 1994. Experimental hints on the fragmentation of the Tunguska Cosmic Body. Planet. Space Sci. 42**,** 777–783.

Skublov, G.T., Marin, Yu.B., Skublov, S.G., Logunova, L.N., Nechaeva, E.S., Savichev, A.A., 2011. Mineralogical-geochemical features of primary rocks, loose sediments and catastrophic mosses in the northern swamp area (region of the Tunguska catastrophe in 1908). Zapiski Ros. Mineral. Soc. 3, 120-138 (in Russian).

Sobotovich, E.V, Kvasnitsa, V.N., Kovalyukh, N.N., Litvin, A.L., Rybalko, S.I, Sharkin, O.P. 1980. Radio-carboniferous and mineralogical evidence of Tunguska body's substance nature. Mineralogical J. 2**,** 36-46 (in Russian).

Sobotovich, E.V., Piven', P.I., Kolesov, G.M., Kostyuchenko, N.G., Kononenko, L.V., Kovalyukh, N.N., 1985. Abundance of some elements in

diamond-graphite growths and other targets from the epicentre of Tunguska disaster. Meteoritika 44**,** 135-138 (in Russian).

Urey, H.C., Mele, A., Mayeda, T., 1957. Diamonds in stone meteorites. Geochim. Cosmochim. Acta 13**,** 1-4.

Valter, A.A., Oleynyk, G.S., Fisenko, A.V., Semenyova, L.F., 2003. Structure-morphological features of apographitic impact formation of diamond from Novo-Urei meteorite. Geokhimiya 10**,** 1027-1035 (in Russian).

Vdovykin, G.P., 1970. Diamonds in meteorites. Publ. House "Nauka", Moscow (in Russian).

Wirth, R., 2004. Focused ion beam (FIB): A novel technology for advanced application of micro- and nanoanalysis in geoscience and applied mineralogy. Europ. J. Mineral. 16**,** 863-876.

Wirth, R., 2009. Focused Ion Beam (FIB) combined with SEM and TEM: Advanced analytical tools for studies of chemical composition, microstructure and crystal structure in geomaterials on a nanometer scale. Chem. Geology 261**,** 217-229.

Yavnel, A.A., 1957. On the composition of the Tunguska meteorite. Geokhimiya 6**,** 553-556 (in Russian).

Zbik, M., 1984. Morphology of the outermost shells of the Tunguska black magnetic spherules. J. Geoph. Research 89**,** 605-611.

Figure captions

Fig.1. Sampling scheme of the sphagnum peat in the epicenter of the Tunguska phenomenon (sampling location is indicated by black circle) (Sobotovich et al., 1980).

Fig.2. SEM images of the Tunguska diamond-lonsdaleite-graphite intergrowths with natural rounded surface (two fragments - a, b) and images of their inner polycrystalline lamellar structure (c, d).

Fig.3. SEM images of troilite (indicated by dark arrows) in carbon matrix of the Tunguska diamond-lonsdaleite-graphite intergrowths: a – hexagonal crystal; b –somewhat rounded hexagonal crystal; c –plate; d – films.

Fig.4. SEM and TEM images of the Tunguska diamond-lonsdaleite-graphite intergrowth: a - SEM image of a fragment, from which the four foils were sputtered (the location indicated by a dark arrow); b - HAADF image of foil # 2532 showing evidence of shock metamorphism – cracks, collapse and fragmentation zones; c – details in image b. Inclusions of troilite and other minerals in cracks; d - dark field image of foil #2522. Nanocrystals forming the carbon matrix as well as indicators of shock compression are discernable.

Fig.5. TEM images of the Tunguska diamond-lonsdaleite-graphite intergrowths: a - SAED pattern of foil #2533, the scattering intensities are attributed to lonsdaleite; b –Inverse FFT image of the high-contrast part of foil #2522 with lattice fringes of diamond and lonsdaleite crystallites; c – EEL spectrum of the carbon C-K edge typical for sp^3 bonding in diamond-lonsdaleite in the foil #2522.

Fig.6. Electron diffraction pattern of the whole foil of apographitic impact diamond: d-spacings (in Å) – 2.17 ($(10\bar{1}0)$ lonsdaleite); 2.06 ((111) diamond and/or (0002) lonsdaleite); 1.26 ((220) diamond and/or $(11\bar{2}0)$ lonsdaleite); 1.079 ((311) diamond and/or $(02\bar{2}0)$ lonsdaleite) and 0.96 ($(20\bar{2}2)$ lonsdaleite.

Fig.7. TEM bright field images of troilite: a – white imperfect crystal (foil #2522); b – bright lamellar crystals (foil #2523).

Fig.8.TEM bright field image of a secretion of troilite, taenite and schreibersite (a, foil #2522) and the corresponding EDX spectra (b, c).

Fig.9. TEM bright field image of FeS (a, foil #2533), corresponding EDX spectra (b) and corresponding SAED pattern (c).

Fig.10. TEM bright field image of taenite (a, foil #2510), corresponding EDX spectra (b) and its SAED pattern (c).

Fig.11. TEM bright field image of γ-Fe (a, foil #2533)) and corresponding EDX spectra (b).

Fig.12. TEM bright field image of schreibersite (a, foil #2510)), corresponding EDX spectra (b) and SAED pattern (c).

Table 1

Interplanar spacings (d in Å) for Tunguska diamond-lonsdaleite-graphite intergrowths [Kvasnitsa et al., 1979]

1*		2*		3*		4*		Graphite**		Diamond**		Lonsdaleite**		Troilite**	
I	d	I	d	I	d	I	d	I	d	I	d	I	d	I	d
4	4.14	2	4.15	2	4.20	3	4.12		-		-		-		-
2	3.69	4	3.72	2	3.74	3	3.74		-		-		-	3	3.82
7	3.32	9	3.30	4	3.36	7	3.35	100	3.36		-		-		-
1	2.96	1	2.95	1	3.02	1	3.00		-		-		-	6	2.968
3	2.69	5	2.65	2	2.68	2	2.65		-		-		-	7	2.644
1	2.39	1	2.42	1	2.43	1	2.52		-		-		-	1	2.531
6	2.30	6	2.30	3	2.30	3	2.31		-		-		-		-
8	2.17	6	2.18	4	2.19	3	2.19	10	2.13		-	100	2.19		-
10	2.067	10	2.072	10	2.087	10	2.080	50	2.03	100	2.06	100	2.06	10	2.085
2	1.930	2	1.940	2	1.953	1	1.926		-		-	50	1.920	4	1.921
2	1.798	1	1.834	2	1.814	2	1.824	5	1.800		-		-		-
2	1.732	2	1.724	1	1.738	2	1.730		-		-		-	2	1.755
	-		-		-		-		-		-		-	9	1.720
4	1.646	6	1.652	3	1.654	3	1.647	80	1.678		-		-	5	1.637
1	1.511	1	1.518	3	1.500	2	1.520	10	1.544		-	25	1.500		-
1	1.474	1	1.460		-	3	1.470		-		-		-	5	1.472
2	1.400	3	1.394	3	1.414	3	1.394		-		-		-	3	1.448
1	1.335	1	1.347		-	2	1.359		-		-		-	8	1.328
8	1.257	8	1.256	6	1.256	5	1.257	30	1.232	25	1.261	75	1.260	6	1.319
2	1.189	3	1.186	1	1.189	2	1.193		-		-		-	4	1.182
	-	1	1.163	1	1.164	1	1.162	50	1.158		-	50	1.170		-
	-	1	1.135		-	1	1.146	20	1.120		-		-		-
5	1.070	5	1.075	3	1.076	5	1.075	16	1.075	16	1.075	25	1.075		-
	-	3	1.000	1	0.999	2	0.998	40	0.994		-		-		-

*1-4 – Tunguska samples. ** The XRDC, 1973.

Table 2

Interplanar spacings (d in Å) for Tunguska samples (foils)

Sample 1, foil #2510-1	Sample 1, foil #2510-2	Sample 1, foil #2522	Sample 2, foil #2523	Graphite*		Lonsdaleite*		Diamond*	
				d	hkil	d	hkil	d	hkl
	3.252		3.304	3.355	0002				
2.168	2.143	2.160	2.167			2.184	$10\bar{1}0$		
2.078		2.090	2.071	2.033	$10\bar{1}1$	2.059	0002	2.059	111
		1.930				1.929	$01\bar{1}1$		
			1.680	1.677	0004				
	1.559					1.498	$10\bar{1}2$		
1.242		1.270	1.250			1.261	$11\bar{2}0$	1.261	220
1.166						1.162	$10\bar{1}3$		

*The JCPDS card, 2003.

Table 3. The chemical composition of taenite (Fe, Ni) occurred from carbon matrix of Tunguska samples (foils), wt. %

Analyses	Fe	Ni
1	84.54	15.46
2	80.14	19.86
3	70.67	29.33

The Fe and Ni contents were acquired with X-ray EDAX system from the FIB-TEM foil.

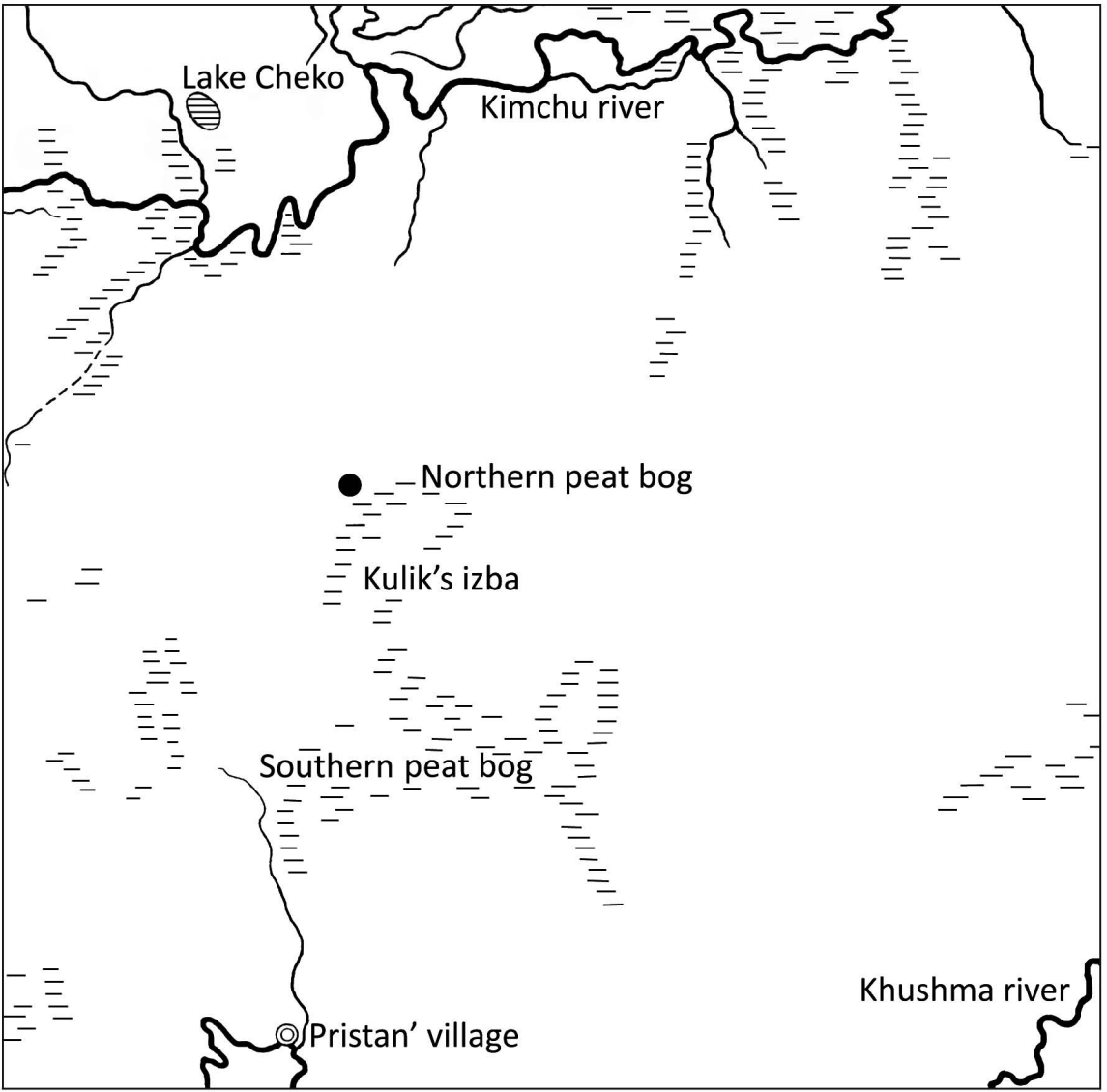
Lake Cheko
Kimchu river
Northern peat bog
Kulik's izba
Southern peat bog
Khushma river
Pristan' village

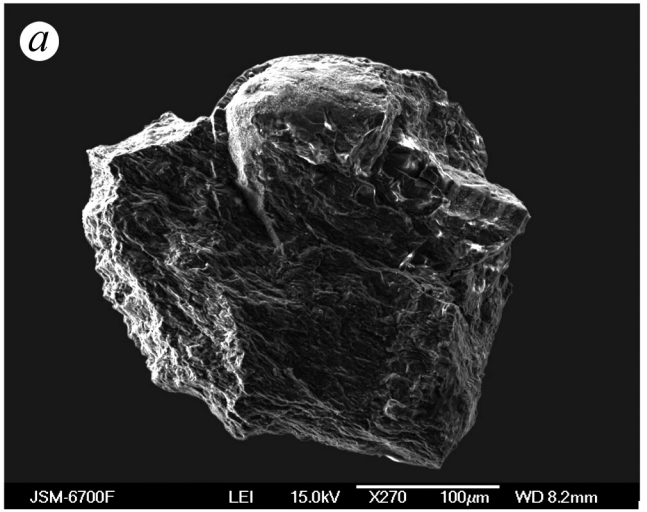
a
JSM-6700F LEI 15.0kV X270 100μm WD 8.2mm

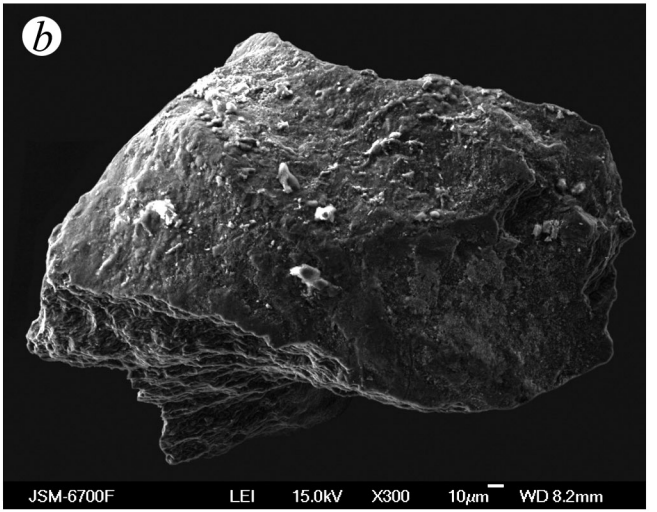
b
JSM-6700F LEI 15.0kV X300 10μm WD 8.2mm

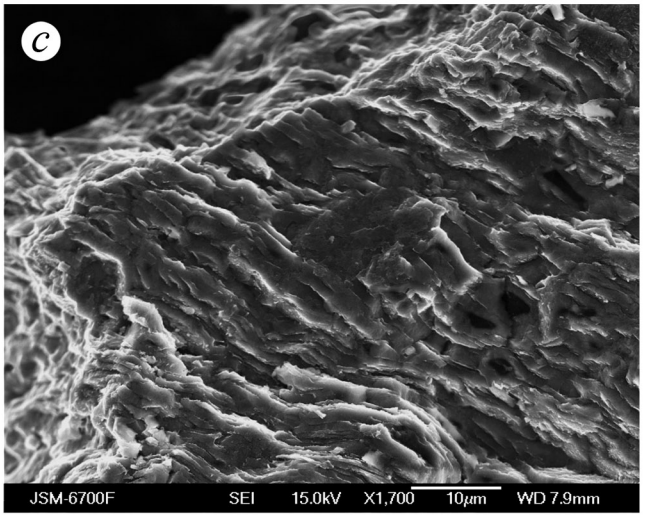
c
JSM-6700F SEI 15.0kV X1,700 10μm WD 7.9mm

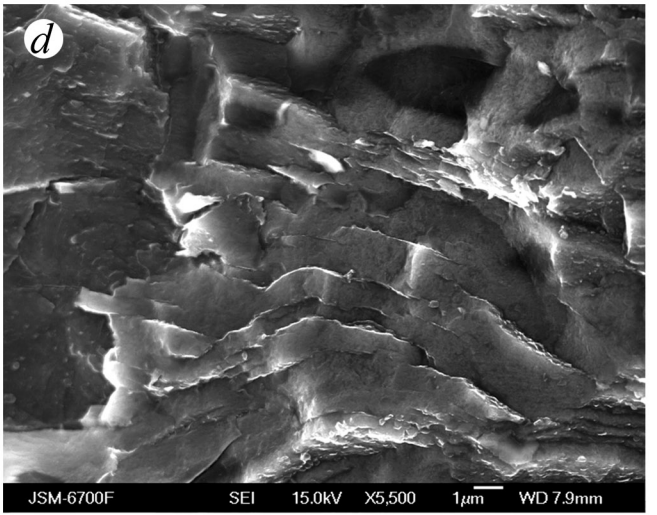
d
JSM-6700F SEI 15.0kV X5,500 1μm WD 7.9mm

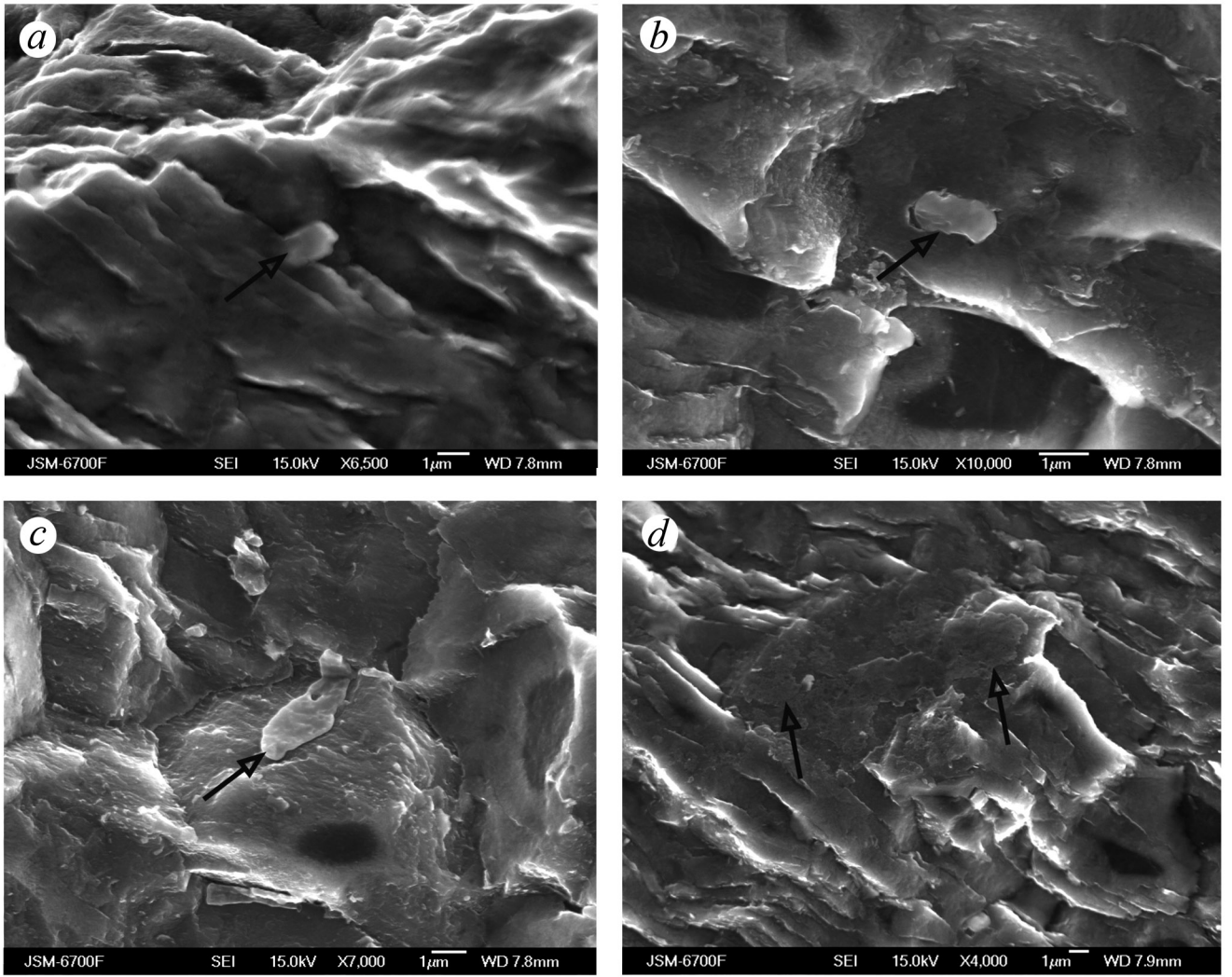
a
JSM-6700F SEI 15.0kV X6,500 1μm WD 7.8mm
b
JSM-6700F SEI 15.0kV X10,000 1μm WD 7.8mm
c
JSM-6700F SEI 15.0kV X7,000 1μm WD 7.8mm
d
JSM-6700F SEI 15.0kV X4,000 1μm WD 7.9mm

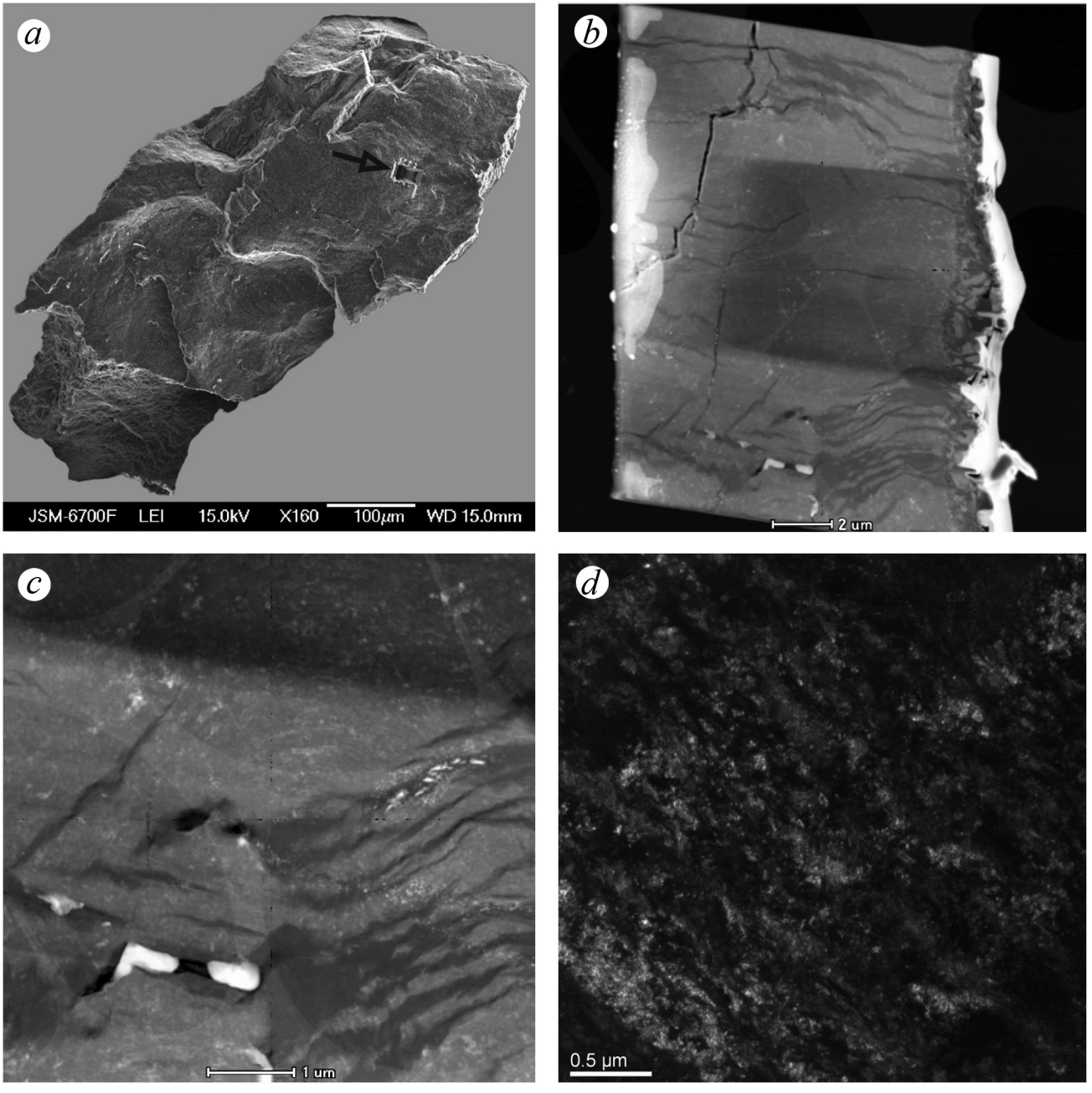
a
JSM-6700F LEI 15.0kV X160 100μm WD 15.0mm
b
2 um
c
1 um
d
0.5 μm

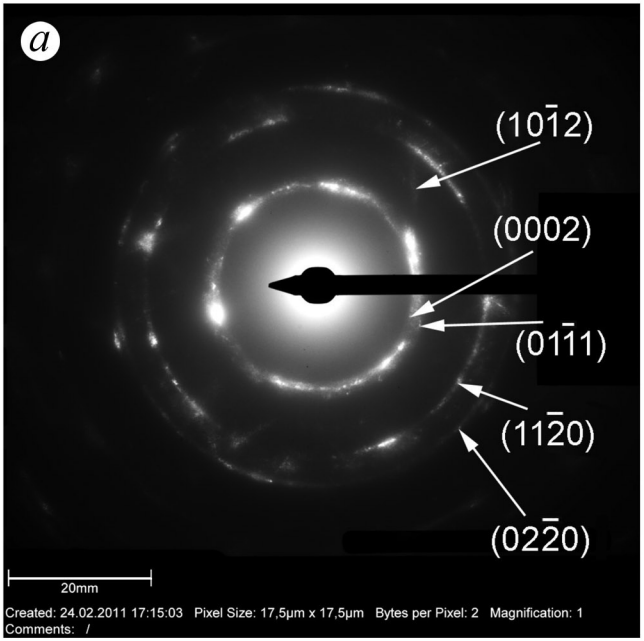
a
(10$\bar{1}$2)
(0002)
(01$\bar{1}$1)
(11$\bar{2}$0)
(02$\bar{2}$0)
20mm
Created: 24.02.2011 17:15:03 Pixel Size: 17,5µm x 17,5µm Bytes per Pixel: 2 Magnification: 1
Comments: /

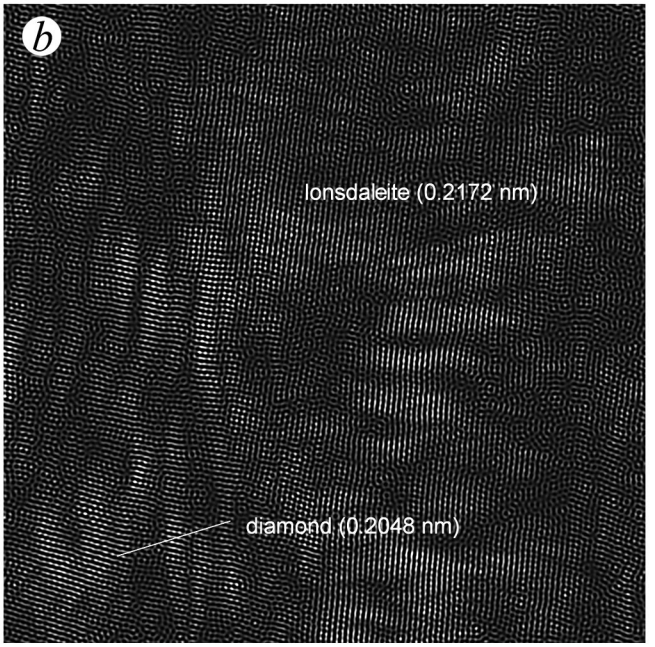
b
lonsdaleite (0.2172 nm)
diamond (0.2048 nm)

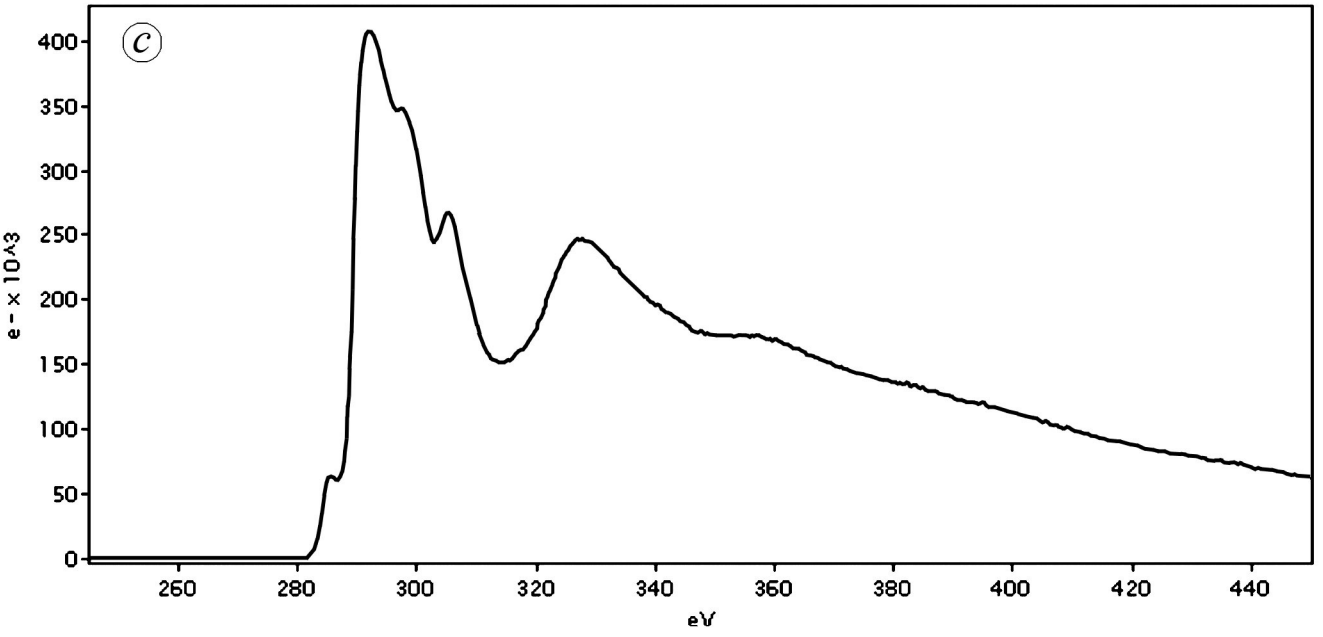
c
e- x 10^3
400
350
300
250
200
150
100
50
0
260
280
300
320
340
360
380
400
420
440
eV

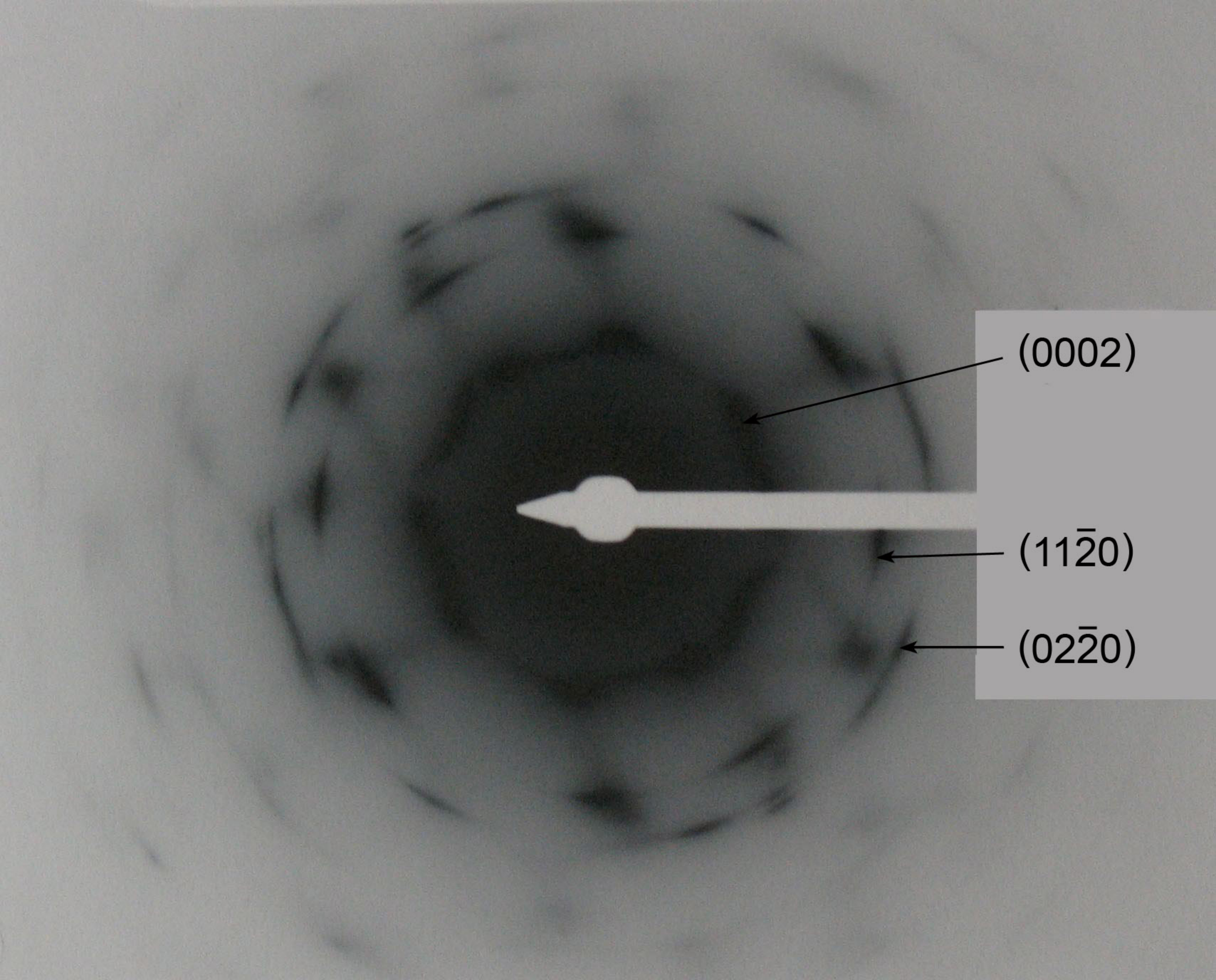
(0002)
(11$\bar{2}$0)
(02$\bar{2}$0)

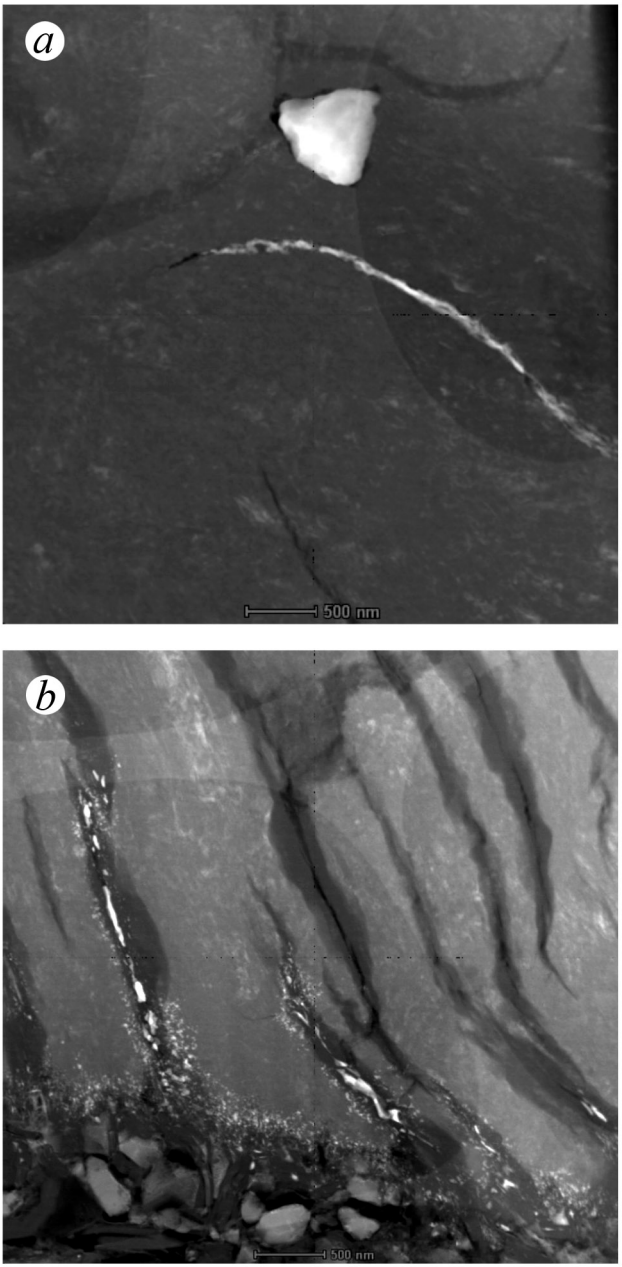
a
500 nm
b
500 nm

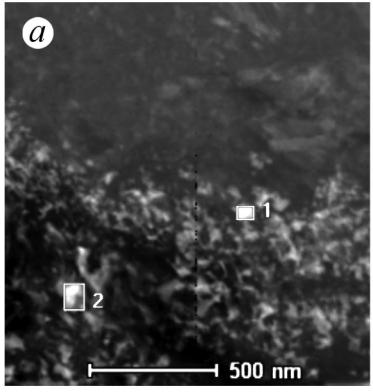
a
1
2
500 nm

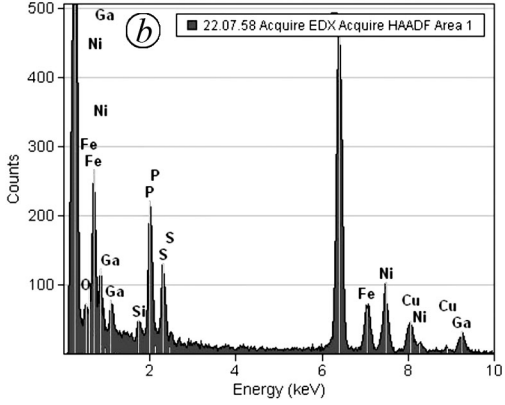
b
22.07.58 Acquire EDX Acquire HAADF Area 1
Counts
Energy (keV)
Ga
Ni
Ni
Fe
Fe
P
P
S
S
Ga
Ga
O
Si
Fe
Ni
Cu
Ni
Cu
Ga

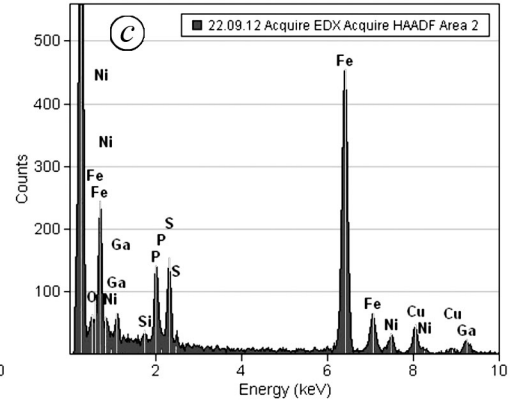
c
22.09.12 Acquire EDX Acquire HAADF Area 2
Counts
Energy (keV)
Fe
Ni
Ni
Fe
Fe
S
P
P
S
Ga
Ga
O
Ni
Si
Fe
Ni
Cu
Ni
Cu
Ga

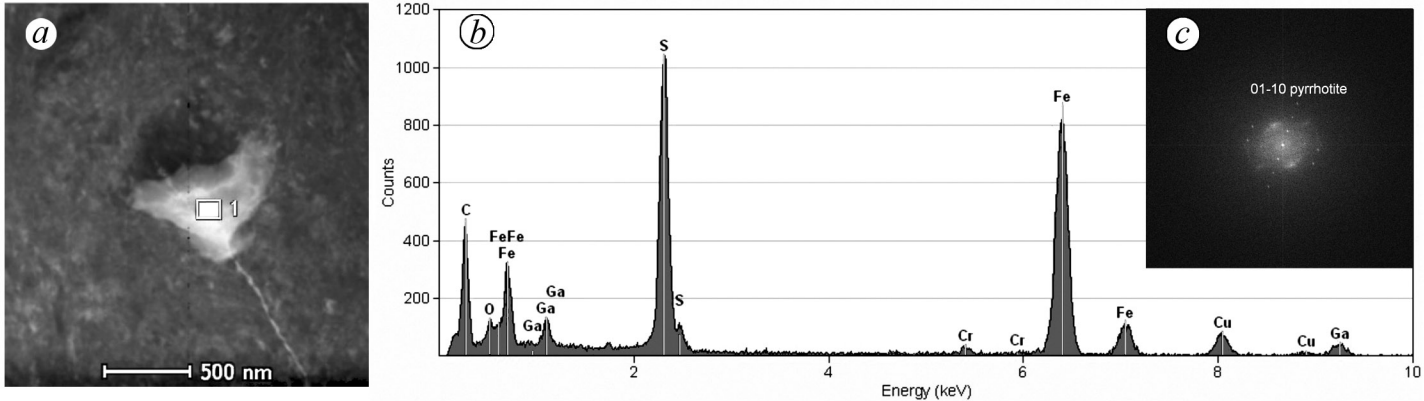
a
1
500 nm
b
Counts
Energy (keV)
C
O
FeFe
Fe
Ga
Ga
Ga
S
S
Cr
Cr
Fe
Fe
Cu
Cu
Ga
c
01-10 pyrrhotite

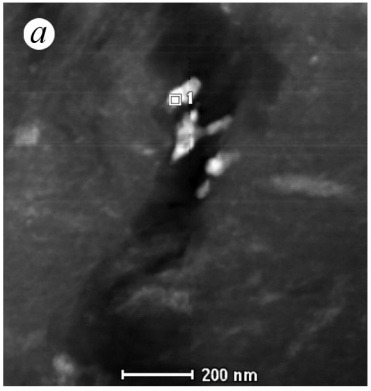
a
1
200 nm

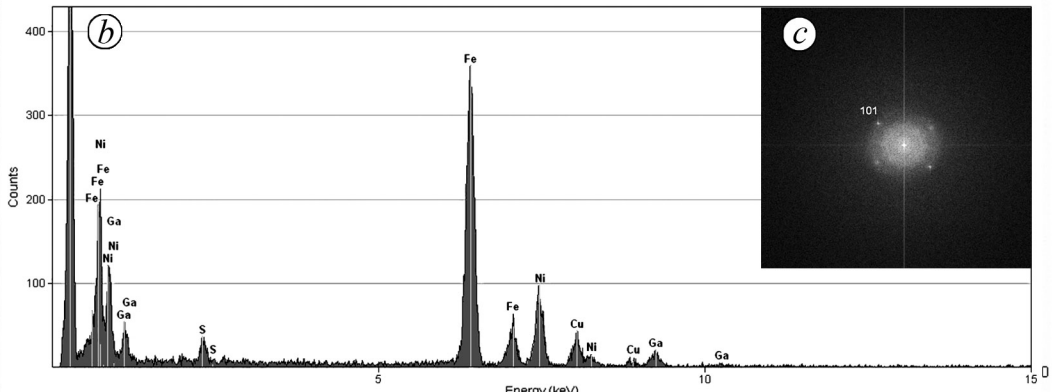
b
Counts
Energy (keV)
Ni
Fe
Fe
Fe
Ga
Ni
Ni
Ga
Ga
S
S
Fe
Fe
Ni
Cu
Ni
Cu
Ga
Ga
c
101

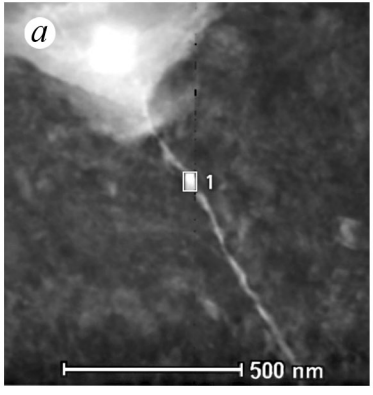
a
1
500 nm

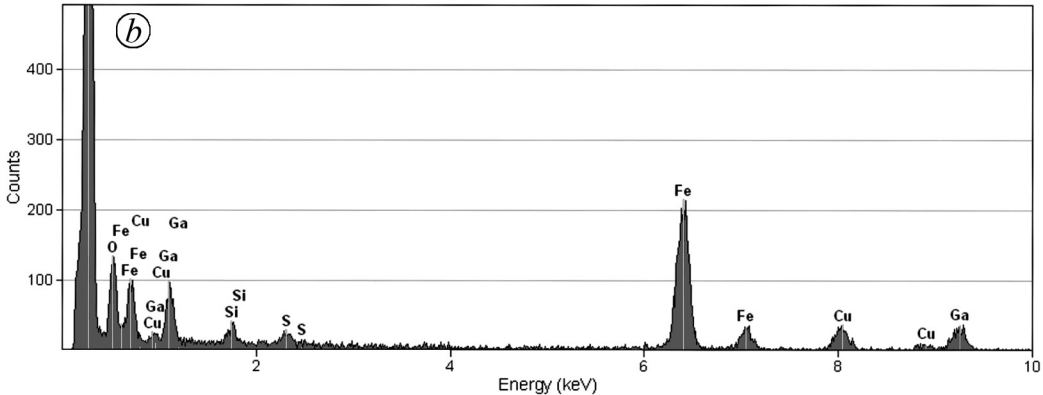
b
Counts
400
300
200
100
O
Fe
Cu
Ga
Fe
Fe
Ga
Cu
Ga
Cu
Si
Si
S
S
Fe
Fe
Cu
Cu
Ga
2
4
6
8
10
Energy (keV)

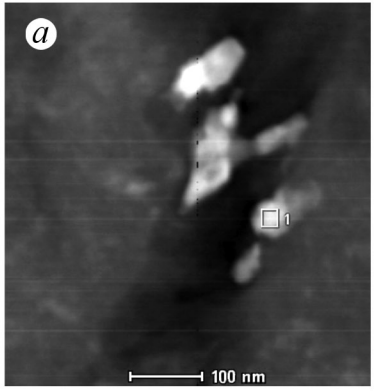
a
1
100 nm

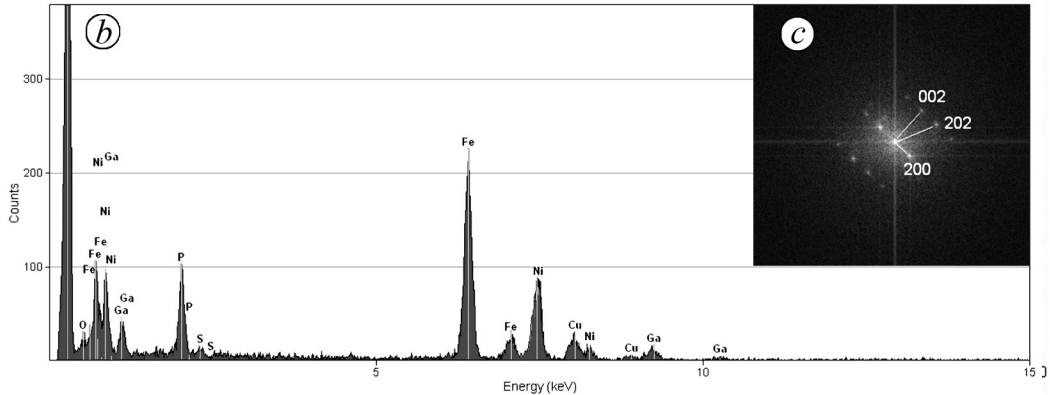
b
Counts
300
200
100
Ni
Ga
Ni
Fe
Fe
Fe
Ni
O
P
P
S
S
Ga
Ga
Fe
Fe
Ni
Cu
Ni
Cu
Ga
Ga
5
10
15
Energy (keV)

c
002
202
200